

Ab Initio Nuclear Structure Calculations of Light Nuclei

Pieter Maris

Department of Physics and Astronomy, Iowa State University, Ames, IA 50011, USA

E-mail: pmaris@iastate.edu

Abstract. We perform no-core configuration interaction calculations for nuclei in the p -shell. We show that for typical light nuclei, a truncation on the total number of quanta in the many-body system converges much more rapidly than a full configuration interaction (FCI) truncation, which is a truncation on the single-particle basis space. We present new results for the ground state energies of the Be isotopes with the nonlocal two-body potential JISP16, and discuss emerging phenomena such as clustering and rotational band structures in ^9Be . We also show that the anomalously suppressed beta decay of ^{14}C to the ground state of ^{14}N can be reproduced using two- and three-nucleon forces from chiral effective field theory. In particular the structure of the ground state of ^{14}N is sensitive to the three-nucleon force.

1. Ab initio nuclear physics

Solving for nuclear properties with the best available nucleon-nucleon (NN) potentials [1, 2], supplemented by three-nucleon forces (3NF) as needed [3, 4, 5], using a quantum many-particle framework that respects all the known symmetries of the potentials is referred to as an "ab initio" problem and is recognized to be computationally hard. Through the UNEDF SciDAC collaboration [6, 7, 8] of nuclear theorists, applied mathematicians, and computer scientists there has been a rapid development of ab initio methods for solving finite nuclei, which has opened a range of nuclear phenomena that can now be evaluated to high precision using realistic inter-nucleon interactions.

A commonly used approach in nuclear physics is the Configuration Interaction (CI) method for solving the many-body nuclear Hamiltonian in a (sufficiently large) single-particle basis space. In this approach, the many-body Schrodinger equation becomes a large sparse matrix problem. The eigenvalues of this matrix are the binding energies, and the corresponding eigenvectors the nuclear wave functions, which can be employed to evaluate experimental quantities. In order to reach numerical convergence for fundamental problems of interest, the matrix dimension often exceeds two billion; obtaining the lowest eigenvalues and eigenvectors of such large sparse matrices poses significant challenges even on today's leadership class facilities.

In this work, we discuss convergence rates of CI calculations, contrasting Full Configuration Interaction (FCI), which is a truncation on the single-particle basis space only, with the N_{max} truncation, which is a truncation on the many-body basis space. The latter is commonly used in nuclear structure calculations, not only because of its superior convergence rate for light nuclei, but also because it leads to an exact separation of the center-of-mass (cm) motion and the translationally-invariant wavefunction.

We use a recently introduced technique for unfolding the cm motion from the one-body density matrices [9], which allows us to obtain translationally-invariant nucleon densities. With this technique we can reveal interesting phenomena such as clustering emerging from our ab initio calculations. In particular we show that the ground state of ^9Be consists of two clusters of protons and neutrons separated by a few fm, consistent with α -cluster models, with the 'extra' neutron forming a ring or donut shape. We also discuss emerging rotational band structure in ^9Be , and present new results for the ground state energies of the beryllium isotopes.

Finally, we discuss recent results for the anomalously long lifetime of ^{14}C , which can be reproduced by the inclusion of three-nucleon forces. We analyse in detail what the influence of the 3NF is, not only on the transition between the ground states of ^{14}C and ^{14}N , but also on the transition between the first excited 2^+ state of ^{14}C and the ground state of ^{14}N . We identify that it is the structure of the ground state of ^{14}N , rather than that of ^{14}C , that responds sensitively to the 3NF, and therefore leads to the anomalously small transition matrix element.

2. No-Core Configuration Interaction calculations of light nuclei

In a no-core CI approach, the wavefunction Ψ of a nucleus consisting of A nucleons (protons and neutrons) is expanded in an A -body basis of Slater Determinants of single-particle states; that is

$$\Psi(\vec{r}_1, \dots, \vec{r}_A) = \sum c_k \Phi_k(\vec{r}_1, \dots, \vec{r}_A), \quad (1)$$

where Φ_k are A -body Slater Determinants. Conventionally, one uses a harmonic oscillator (HO) basis for the single-particle states, but it is straightforward to extend this approach to a more general single-particle basis [10].

We use the so-called M -scheme for our basis. The single-particle states are labelled by the quantum numbers n , l , j , and m_j , where n and l are the radial and orbital HO quantum numbers, with $N = 2n + l$ the number of HO quanta; j is the total single-particle spin, and m_j its projection along the z -axis. The many-body basis states have well-defined total spin-projection, which is simply the sum of m_j of the single-particle states, $M_j = \sum m_j$, hence the name M -scheme. However, in general the many-body basis states do not have a well-defined total J . Some of the advantages of this scheme is that it is very simple to implement, and that in two runs (for positive and negative parity), we get the complete low-lying spectrum, including the ground state, even if we do not know what the spin of the ground state is.

The interaction V , typically a two-body (NN), sometimes supplemented by a three-body (3NF) potential, is also expressed in this many-body basis, as is the kinetic energy T . Diagonalizing the resulting matrix $H = T + V$ gives us the eigenstates and eigenenergies. In general, we are only interested in the low-lying spectrum, so we do not need a complete diagonalization of this matrix, which can be rather large, exceeding 12 billion basis states in a recent application.

2.1. Truncation and Convergence

In principle, by expanding the nuclear wavefunction in a complete basis, we would obtain exact results for a given input interaction V . However, such a basis is infinite-dimensional, and practical calculations can only be done in a finite-dimensional truncation of a complete basis. In order to recover exact results, independent of the basis space truncation, we typically perform a series of calculations in increasingly large basis spaces. Based on the results of such a series of calculations, we either find that we have achieved numerical convergence (within a certain numerical uncertainty), or extrapolate to the complete basis (with a certain extrapolation uncertainty). Of course, for some observables it is much harder to achieve convergence than for others, as we shall see. In addition, one could employ renormalization techniques to accelerate convergence in relatively small basis spaces.

Full Configuration Interaction or FCI employs a widely-known truncation in which all many-body basis states are retained that can be constructed from a finite set of single-particle states. This method is commonly used in atomic and molecular physics.

In ab initio nuclear physics however, we generally use a truncation on the many-body basis space, rather than on the single-particle basis. To be specific, we construct a finite-dimensional basis by a truncation on the total number of quanta of the system. That is, the many-body basis for a nucleus consisting of A nucleons is limited to states that satisfy the condition

$$\sum_{k=1}^A N_k \leq N_0 + N_{\max}, \quad (2)$$

where N_k is the number of quanta of each of the single-particle states in the many-body basis state; N_0 is the minimal number of quanta for that nucleus; and N_{\max} is the truncation parameter. For HO single-particle states, or more general, for any basis in which the single-particle states have radial and orbital quantum numbers n and l , we have $N_k = 2n_k + l_k$.

There are several advantages to this N_{\max} truncation. One is that, in combination with a HO basis for the single-particle basis, it leads to an exact factorization of the cm motion and the relative motion. In nuclear physics, we deal with a self-bound system, and we have to either use relative coordinates for our calculations, or (as we do here) single-particle coordinates. Note that the wavefunctions in Eq. (1) are functions of A (independent) single-particle coordinates, not $(A - 1)$ relative coordinates. This makes the anti-symmetrizations and bookkeeping in the numerical codes almost trivial, but it does mean that we have to somehow separate out the cm wavefunction from the translationally-invariant wavefunction. A HO single-particle basis, in combination with N_{\max} truncation, allows for an exact factorization of the cm wavefunction

$$\Psi(\vec{r}_i) = \Psi_{\text{cm}}^{\omega}(\vec{R}) \otimes \Psi_{\text{ti}}, \quad (3)$$

where $\vec{R} = (\frac{1}{A}) \sum_{i=1}^A \vec{r}_i$ and Ψ_{ti} does not depend on the cm motion. In order to remove the states with cm excitations from the low-lying spectrum, we use the Lawson method [11] whereby we add a Lagrange multiplier term, $\lambda(H_{\text{cm}}^{\omega} - \frac{3}{2}\hbar\omega)$, to the many-body Hamiltonian. The actual Hamiltonian that we are using thus takes the form

$$H^{\lambda,\omega} = T_{\text{rel}} + \lambda_{\text{cm}} \left(H_{\text{cm}}^{\text{HO}} - \frac{3}{2}\hbar\omega \right) + \sum_{i < j} V_{ij} + \sum_{i < j < k} V_{ijk} + \dots \quad (4)$$

Note that although this Hamiltonian depends explicitly on the HO parameter $\hbar\omega$, as well as on λ , the low-lying spectrum (i.e. states with $E_{\text{excitation}} \lesssim \lambda\hbar\omega$) only depends implicitly on $\hbar\omega$ through the basis space truncation, and becomes independent of $\hbar\omega$ in the infinite-basis limit.

In the infinite-basis limit both FCI and the N_{\max} truncations should converge to the same exact result. It turns out that the numerical convergence is significantly faster with an N_{\max} truncation than with an FCI truncation [12, 13] in our nuclear physics applications. In Fig. 1 we compare the convergence rate for two light nuclei, ^4He and ^6Li , with an FCI truncation and with an N_{\max} truncation. These calculations were performed with a realistic two-body interaction derived from inverse scattering theory, JISP16 [14], which has been demonstrated to have good convergence rates for the ground state energies of nuclei with $A \leq 16$ [15]; and it gives a good description of light nuclei without explicit three-body forces.

The left panel of Fig. 1 shows that for ^4He both FCI and the N_{\max} truncation have a similar convergence rate, at least in terms of the HO parameter $\hbar\omega$ and the truncation parameter N_{shell} and N_{\max} respectively. As the truncation parameter increases, the dependence on $\hbar\omega$ decreases, and the successive N_{shell} curves (dotted) and N_{\max} curves (solid) converge to the same ground state energy of -28.299 MeV.

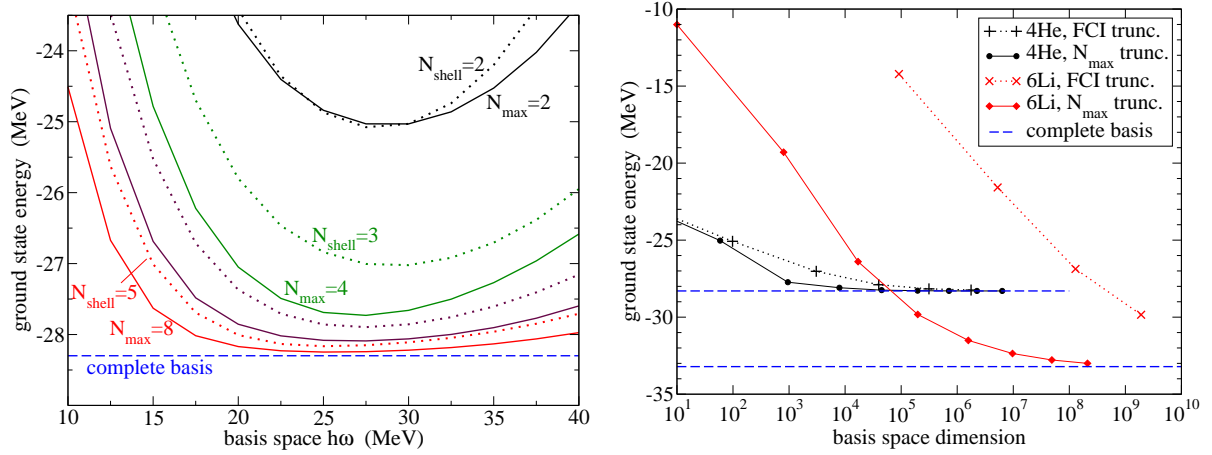


Figure 1. Comparison of the convergence rates with JISP16 using FCI (dotted) and N_{max} truncations (solid). Left: the ground state energy of ^4He as function of $\hbar\omega$; Right: the ground state energies of ^4He and ^6Li as function of the basis space dimension. The dashed line represents the exact result in a complete basis.

However, as function of the basis space dimension, the N_{max} truncation converges much more rapidly than the FCI calculations, as is illustrated in the right panel of Fig. 1. E.g., an $N_{\text{max}} = 8$ calculation with a basis dimension of less than 50,000 for ^4He leads to a ground state energy that is well within 100 keV of the exact result, whereas for an FCI calculation $N_{\text{shell}} = 6$ with a basis dimension of almost 2 million is needed in order to achieve a similar level of convergence. For ^6Li , an FCI calculation with a basis dimension of over a billion is still more than 3 MeV from the exact ground state energy, whereas an $N_{\text{max}} = 10$ calculation with a basis dimension of about 10 million is within 1 MeV of the converged ground state energy. Also for other observables [13], such as radii and quadrupole moments, the convergence seems to be slower with the FCI truncation than with the N_{max} truncation, when viewed as function of the basis space dimension.

Finally, with the N_{max} truncation one may easily separate the positive parity spectrum and the negative parity spectrum. Two successive shells have opposite parity, depending on whether the orbital angular momentum is even or odd. By increasing the total number of quanta of the many-body basis states by two quanta at a time, we automatically create a basis with a specific parity. The 'natural' parity of a nucleus is given by its valence space, for which our calculations start with $N_{\text{max}} = 0$; for the 'unnatural' parity spectrum we would perform a series of calculations starting with $N_{\text{max}} = 1$. In both cases, N_{max} is increased by two quanta as we increase the basis space. (Of course, it is straightforward to include a parity-constraint in FCI calculations, and in fact, the dimensions given here for FCI calculations do incorporate such a constraint.)

2.2. Extrapolation to the complete basis

For a very light nucleus like ^4He or ^6Li one can achieve convergence of the ground state energy and other observables by simply going to a sufficiently large basis, but for larger nuclei that is not practical. However, based on a series of calculations in finite basis spaces, we can extrapolate those results to a complete, infinite-dimensional, basis. Empirically [15, 16] the nuclear binding energies seem to converge exponentially with N_{max}

$$E_{\text{binding}}^N = E_{\text{binding}}^\infty + a_1 \exp(-a_2 N_{\text{max}}). \quad (5)$$

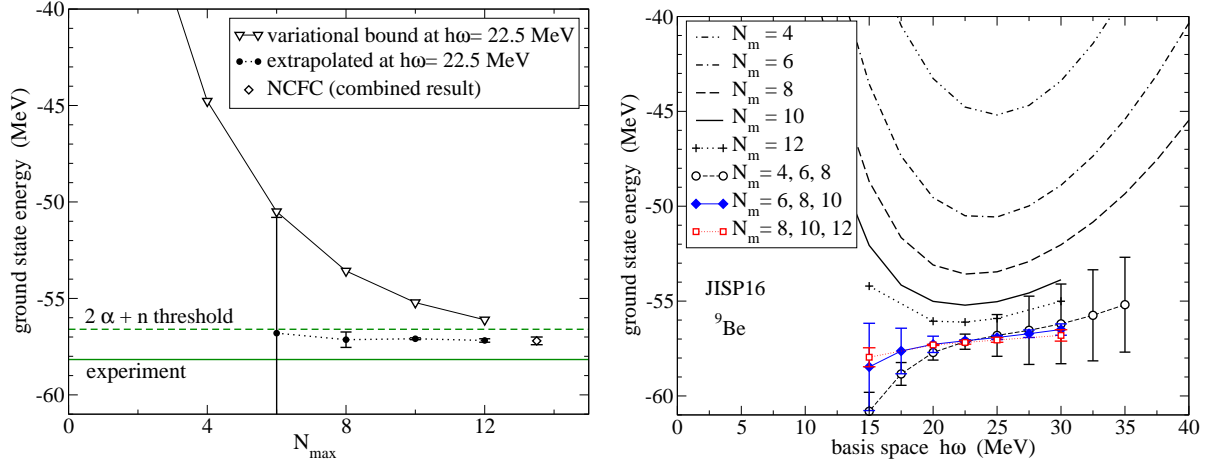


Figure 2. Ground state energy of ${}^9\text{Be}$ with JISP16 as function of N_{\max} (left) and as function of $\hbar\omega$ for several N_{\max} values (right), as well as extrapolated results with error estimates.

There are several different ways in which one can exploit this (empirical) convergence behavior. Here we use three consecutive N_{\max} values at a fixed basis space parameter $\hbar\omega$ in order to estimate a converged binding energy at that $\hbar\omega$. Under the assumption that the convergence is indeed exponential, such an extrapolation should get more accurate as N_{\max} increases; the difference between the extrapolated results from two consecutive sets of three N_{\max} values is then used as an estimate of the numerical uncertainty associated with the extrapolation. We do this for a range of basis space $\hbar\omega$ values, in order to check the consistency of the extrapolated results and their error estimates. (We only use three consecutive N_{\max} values for each extrapolation, since our results at finite basis spaces are accurate to at least five significant figures.)

This procedure is illustrated for ${}^9\text{Be}$ in Fig. 2, again with JISP16. In the left panel we show the ground state energy for a series of calculations at a fixed HO parameter $\hbar\omega$, as well as the extrapolated ground state energy. For the error estimate on the first extrapolated value, obtained from calculations at $N_{\max} = 2, 4$, and 6 , we use the difference between the calculated result at $N_{\max} = 6$ and the extrapolated value; for higher N_{\max} values we use the difference with the value obtained from the next-smaller basis spaces.

The extrapolated result appears to be very well converged (i.e. consistent within diminishing errors) starting from $N_{\max} = 8$, not only as function of N_{\max} , but also as function of the basis space parameter $\hbar\omega$, as can be seen from the right panel of Fig. 2. For our final No-Core Full Configuration (NCFC) result we combine the extrapolation results for a range of HO parameters at and slightly above the variational minimum to arrive at our best estimate for the results in the complete basis, independent of all basis parameters.

2.3. Need for HPC and Code performance

In order to reliably extrapolate to the complete basis, we need results in finite bases up to at least $N_{\max} = 8$ (9 for unnatural parity states), and preferably $N_{\max} = 10$ (11 for unnatural parity states) or higher. This leads to a computational challenge, because the basis space dimension increases rather rapidly with N_{\max} and with the number of particles. Furthermore, the sparsity of the matrix depends on the 'rank' of the potential: a two-body potential leads to a much sparser many-body matrix than a three-body potential.

In Fig. 3 we show the basis space dimensions for a number of $N = Z$ nuclei in the p -shell (solid curves), as well as a few nuclei in the sd -shell. The basis space dimension for even the first couple of nuclei in the sd -shell (more than 8 protons and 8 neutrons) is of the order of 10 billion or more

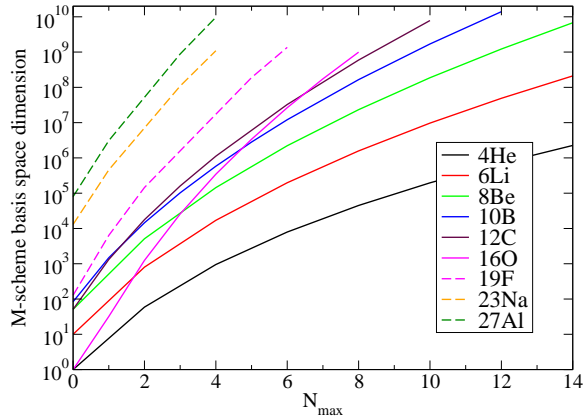


Figure 3. Basis space dimension as function of N_{\max} for $N = Z$ nuclei in the p -shell (solid), as well as a few nuclei in the sd -shell (dashed).

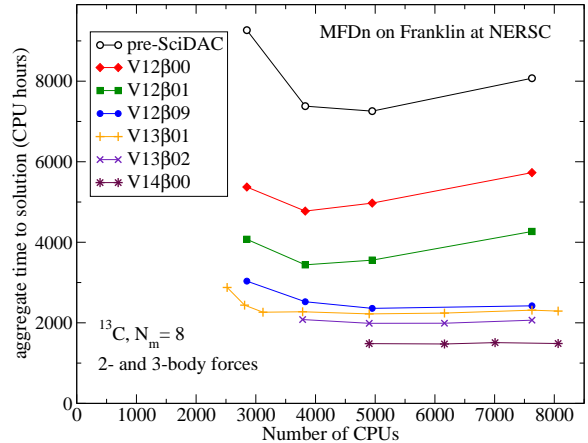


Figure 4. Performance improvements on Franklin (at NERSC) of the code MFDn for ^{13}C with 2- and 3-body forces.

at $N_{\max} = 8$. As the matrix size increases, there is a clear need for high-performance computing: obtaining the lowest 10 to 20 eigenvalues and eigenvectors of matrices with a dimension of the order of several billion is a nontrivial task, even if the matrix is extremely sparse.

For our calculations we use the code MFDn, which is a hybrid MPI/OpenMP parallel Fortran 90 code for nuclear structure calculations, that has been in development for over two decades. Significant improvements in its performance have been made over the last four years [17, 18, 19] under the UNEDF SciDAC program, as is illustrated in Fig. 4. On currently available machines, the largest many-body basis dimension that MFDn can handle is about 10 to 15 billion with two-body forces only, and about one billion with two- and three-body forces.

MFDn constructs the many-body basis states in M -scheme and the corresponding Hamiltonian matrix, and solves for the lowest eigenstates using an iterative Lanczos algorithm. At the end of a run, it writes the nuclear wavefunctions to file, and evaluates selected physical observables which can be compared to experimental data (the wavefunctions themselves are not experimentally observable). It also writes out the one-body density matrix elements (in the underlying single-particle basis), which can be used for further analysis.

The matrix is distributed in a 2-dimensional fashion over the processors, and we work with the lower triangle only, because the matrix is symmetric (and real). Because of the 2-dimensional distribution of the matrix, it runs on $n(n+1)/2$ processors, where n is the number of “diagonal” processors. Both the memory usage and the (local) CPU usage are distributed evenly over all processors. This load-balancing is achieved by a round-robin distribution of the M -scheme basis states over the “diagonal” processors. The disadvantage of this scheme is that it destroys any natural sparsity structure in the matrix. We are currently working on a new load-balancing scheme that retains some of the natural sparsity structure (Version 14 in Fig. 4). The Lanczos vectors are also stored in memory, distributed over all processors; this allows for fast and efficient re-orthogonalization after every matrix-vector multiplication. Note that the re-orthogonalization is done in double precision, even though the matrix and vectors themselves are stored in single precision. This turned out to be essential in order to maintain numerical accuracy over hundreds of Lanczos iterations with matrix dimensions in the billions.

The code has good scaling characteristics, as illustrated by the flatness of the curves for the more recent versions of the code in Fig. 4. For large runs on modern multi-core architectures such as the Cray XT4/5 and XE6, it is significantly more efficient to run the code in a hybrid mode, using OpenMP threading within a node, and MPI between nodes [19]. We are currently working

on improving the performance on NUMA architectures by focussing on the data locality [20].

The increase in aggregate CPU time as the number of CPUs goes below 4,000 in Fig. 4 is due to the memory limitations. One of the recent code developments was focussed on reducing the memory footprint by partially re-generating the matrix 'on the fly'. This enabled us to perform the largest runs with two- and three-body forces for ^{14}C and ^{14}N on Jaquar at ORNL [21].

3. Emergence of clustering and rotational phenomena in Beryllium isotopes

Among the Be-isotopes there are several interesting and challenging problems for ab initio nuclear structure calculations: α -clustering is likely to play an important role, in particular for ^8Be and ^9Be ; there are several rotational bands; and they are among the lightest nuclei for which both positive and negative parity states are known experimentally. With the NCFC approach described above, we should be able to perform reasonably accurate calculations for the Be-isotopes from ^6Be up to ^{12}Be , provided we use a suitably soft interaction such as JISP16.

3.1. Clustering

We have already presented our results for the ground state energy of ^9Be in Fig. 2. With JISP16 we find a ground energy of $E_{\text{gs}} = -57.2(2)$ MeV, compared to an experimental value of $E_{\text{gs}} = -58.167$ MeV, that is JISP16 underbinds ^9Be by about 1 MeV. Despite this underbinding, our result is below the threshold for two α particles (plus a neutron), which is at -56.6 MeV. Thus we are dealing with a true bound state, not a resonance state.

The next question that naturally arises is: what is the structure of this state? In particular, does it have a structure of two α particles plus a neutron, as one might expect? In an attempt to answer such questions, we have looked at the proton and neutron densities in coordinate-space.

The local density for a nucleus with wavefunction Ψ is given by

$$\rho(\vec{r}) = \int \Psi^*(\vec{r}, \vec{r}_2, \dots, \vec{r}_A) \Psi(\vec{r}, \vec{r}_2, \dots, \vec{r}_A) d^3r_2 \dots d^3r_A. \quad (6)$$

This corresponds to the probability of finding a nucleon at position \vec{r} . Since we use a basis in single-particle coordinates, rather than relative coordinates, our wavefunction $\Psi(\vec{r}_i)$ includes cm motion. The local density extracted from such wavefunctions therefore includes also contributions from the cm motion. However, because of the exact factorization of the cm wavefunction, see Eq. (3), this density is a convolution of the cm density and a translationally-invariant density ρ_{ti} relative to the cm of the entire nucleus

$$\rho^\omega(\vec{r}) = \int \rho_{\text{ti}}(\vec{r} - \vec{R}) \rho_{\text{cm}}^\omega(\vec{R}) d^3R. \quad (7)$$

The cm density ρ_{cm}^ω is a simple Gaussian that smears out ρ_{ti} and obfuscates details of the local density¹. The translationally-invariant density ρ_{ti} can be obtained by a deconvolution of the cm density using standard Fourier methods [9]

$$\rho_{\text{ti}}(\vec{r}) = F^{-1} \left[\frac{F[\rho^\omega(\vec{r})]}{F[\rho_{\text{cm}}^\omega(\vec{r})]} \right], \quad (8)$$

where $F[f(\vec{r})]$ is the 3D Fourier transform of $f(\vec{r})$. Note that the densities on the RHS of this equation depend on the basis space parameter $\hbar\omega$, even in the infinite-basis limit, but the LHS is independent of the basis in this limit.

¹ Note that the cm motion also introduces a spurious dependence on the basis parameter $\hbar\omega$ into ρ^ω that masks the convergence. Even in the limit of a converged calculation in a complete basis, ρ^ω depends on $\hbar\omega$, whereas the translationally-invariant density ρ_{ti} becomes independent of the basis as one approaches convergence.

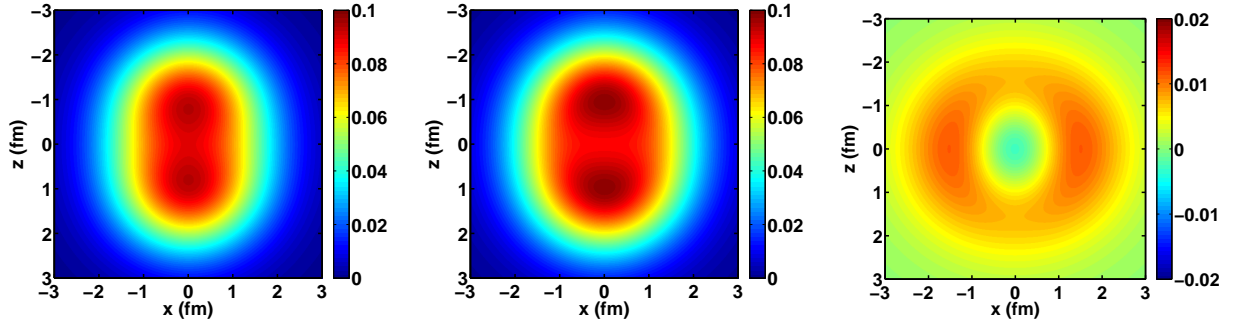


Figure 5. Proton (left), neutron (center), and the difference between the neutron and proton density (right) for the $J^\pi = \frac{3}{2}^-$ ground state of ^9Be , with $M_j = \frac{3}{2}$ using JISP16.

In Fig. 5 we show the proton and neutron densities for the $J^\pi = \frac{3}{2}^-$ ground state of ^9Be , with $M_j = \frac{3}{2}$, obtained with JISP16 in a $N_{\text{max}} = 10$, $\hbar\omega = 12.5$ MeV basis space, where the RMS radii seem to be most converged. The spurious cm contribution has been removed as described above producing the translationally-invariant neutron and proton densities shown in Fig. 5. The figure shows the density in the xz -plane, and is symmetric along the z -axis (vertical axis). It clearly shows a clustering of both the protons and the neutrons into two compact dense regions, separated by about 2 fm along the z -axis. Although this does not prove that we have α -clustering in our ab initio calculation, it is at least consistent with α -clustering. Furthermore, the difference of the neutron and proton density (right panel of Fig. 5) shows that the 'extra' neutron forms a ring or donut shape around the z -axis, rather than being centered in between the dominant proton and neutron clusters.

3.2. Rotation

Rotational bands arise quite naturally in α -cluster models for the Be isotopes [22], so now that we do see some evidence for clustering in ^9Be , we can also expect the corresponding rotational states in the spectrum. The rotational energy for states in a rotational band with an axial symmetry is given by [23]

$$E_{\text{rotational}} = \frac{\hbar^2}{2\mathcal{I}} (J(J+1) - K^2), \quad (9)$$

where \mathcal{I} is the moment of inertia, K is the projection of J along the intrinsic symmetry axis, and J is the total angular momentum. Thus rotational bands show up as straight lines if we plot the excitation energies as function of $J(J+1)$.

For the ground state rotational band in ^9Be we have $K = J = \frac{3}{2}$. Indeed, the spectrum shown in the left panel of Fig. 6 suggests that the lowest $J = \frac{5}{2}$, $J = \frac{7}{2}$, and $J = \frac{9}{2}$ states form a rotational band with the ground state. Furthermore, the excitation energy of the members of this rotational band is very well converged, in particular for the $J = \frac{5}{2}$ and $J = \frac{7}{2}$ states. The calculated excitation energy also agrees quite well with the experimental spectrum, though we do predict a $J = \frac{9}{2}$ member of this rotational band, in addition to the confirmed experimental $J = \frac{5}{2}$ and $J = \frac{7}{2}$ states.

The spectrum by itself is not sufficient to claim that these states are indeed rotational states. The rotational model also predicts the quadrupole moments of a rotational band to all be related to an 'intrinsic' quadrupole moment Q_0 [23]

$$Q(J) = \frac{3K^2 - J(J+1)}{(J+1)(2J+3)} Q_0. \quad (10)$$

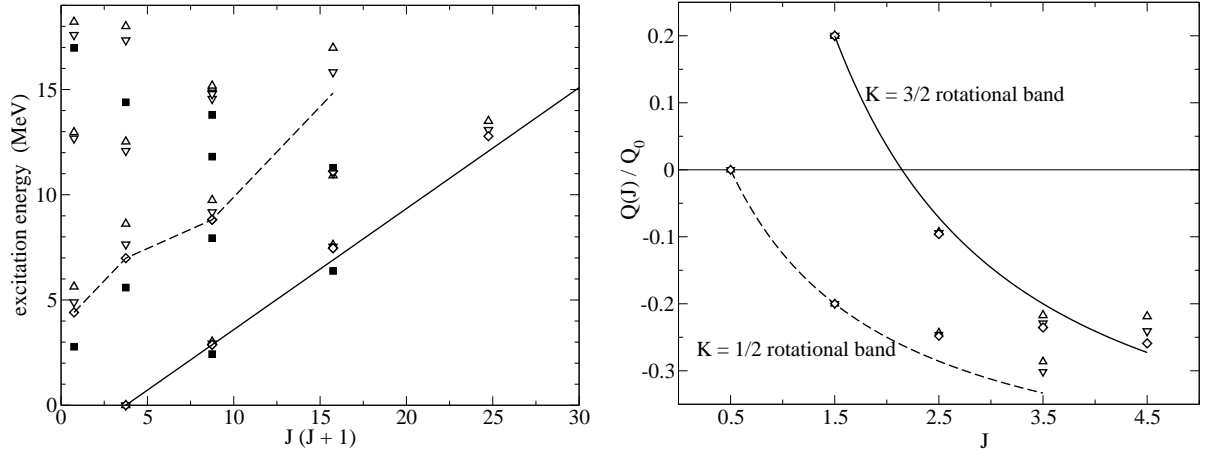


Figure 6. Evidence for the ground state $K = 3/2$ (—) and excited $K = 1/2$ (- - -) rotational bands in ${}^9\text{Be}$ from ab initio calculations with JISP16 (Δ : $N_{\text{max}} = 8$, ∇ : $N_{\text{max}} = 10$, \diamond : $N_{\text{max}} = 12$) Left: Negative parity spectrum as function of $J(J+1)$ (\blacksquare : experimental data from Ref. [25].); Right: Quadrupole moments of the rotational bands normalized by Q_0 .

The strength of the $B(E2)$ transitions within a rotational band also follow from this intrinsic quadrupole moment Q_0 . Even though the quadrupole moments are not very well converged in our calculations², the *ratio* of the quadrupole moments does seem to be reasonably well converged. In the right panel of Fig. 6 we show the quadrupole moments, normalized by the intrinsic quadrupole moment, Q_0 , extracted from the ground state. They agree quite well with the prediction of Eq. (10). Also the calculated $B(E2)$ transitions are in reasonable agreement with the rotational model [24].

The other states in the low-lying negative-parity spectrum of ${}^9\text{Be}$ are not as well converged as the ground state rotational band, as can be seen from the left panel of Fig. 6. However, our calculations suggests that there is also a $K = \frac{1}{2}$ rotational band, starting from the first $J = \frac{1}{2}$ state. Note that it involves the third $J = \frac{7}{2}$ state, rather than the second. Not only are the excitation energies in agreement with predictions from a rotational model (including the staggering due to the Coriolis effect), the quadrupole moments also agree with Eq. (10). In addition, the convergence pattern of these four states is quite similar. The lowest three states of this band seem to converge towards the experimental excitation energies. More work is needed to determine whether these states indeed form a rotational band [24].

3.3. Ground state energies and parity splittings

With JISP16 we have not only looked at ${}^9\text{Be}$, but also at the other Be-isotopes, from ${}^6\text{Be}$ up to ${}^{14}\text{Be}$. Because of the variational principle, any result for the ground state energy in a finite basis truncation forms a strict upper bound for the exact ground state energy. Indeed, our calculated energies in finite basis spaces tend to be well above the experimental ground state energies, see Fig. 7. With an exponential extrapolation on the total binding energies we obtain results for the ground state energies (with numerical error bars due to the extrapolation uncertainties) that are in general much closer to the experimental ground state energies than these variational upper bounds. It turns out that with JISP16 all Be-isotopes are underbound (left panel of Fig. 7): the light isotopes, ${}^6\text{Be}$ and ${}^7\text{Be}$, by a fraction of an MeV, and the neutron-rich isotopes ${}^{13}\text{Be}$ and

² The HO basis functions fall off like $\exp(-r^2)$ whereas the asymptotic behavior of the nuclear wavefunction is known to be an exponential, $\exp(-r)$, rather than a Gaussian. The quadrupole moments are sensitive to this long-range part of the nuclear wavefunction that is not very well represented in a finite HO basis.

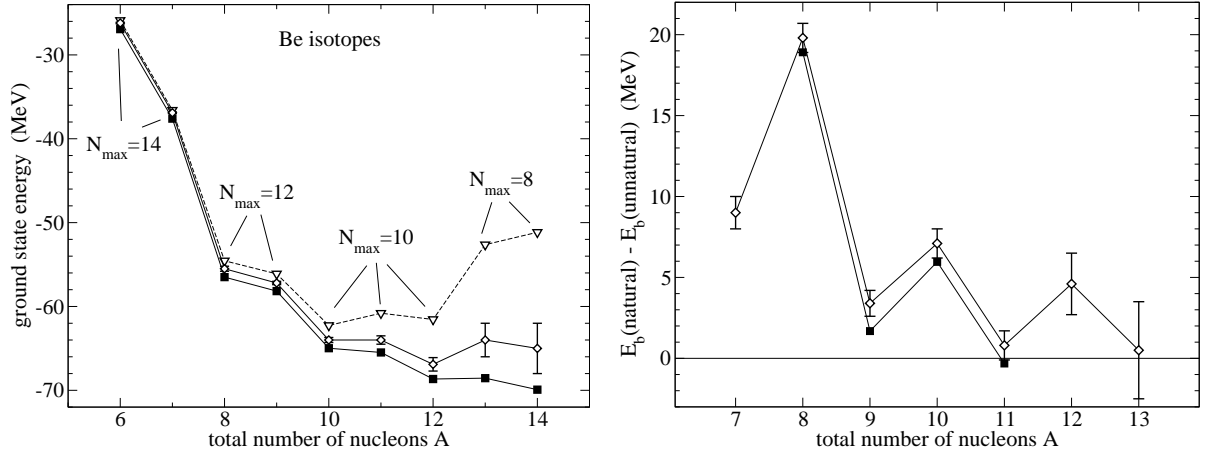


Figure 7. Ground state energies (left) and parity splittings (right) of Be-isotopes with JISP16 (variational upperbound: ∇ , NCFC: \diamond), together with experimental data (\blacksquare) from Refs. [25, 26].

^{14}Be , by about 5 MeV. Nevertheless, the overall pattern of the ground state energies is in quite good agreement with the data. Also the spectra and several other observable quantities do seem to be in quite good agreement with the data, despite this overall underbinding.

Starting with ^8Be , states of both parities appear in the low-lying spectrum; and for ^{11}Be the lowest positive parity state is the ground state, contrary to the expectations based on the shell model, which predicts negative parity ground states for all odd p -shell nuclei. For ^7Be through ^{13}Be we performed our calculations for both natural parity states and for unnatural parity states. We then perform independent extrapolations for the lowest positive parity states and the for the lowest negative parity states.

In the right panel of Fig. 7 we show the difference between the binding energy of the lowest natural parity state and the lowest unnatural parity state. For most isotopes we expect this difference to be positive, but for isotopes with parity inversion it becomes negative. Although our results do not quite reproduce the observed parity inversion for ^{11}Be , parity inversion is within our numerical error estimates for this isotope. Furthermore, over the range of isotopes from ^8Be to ^{11}Be our results are in very good qualitative agreement with the data: with JISP16 we seem to underbind all unnatural parity states by a similar amount of about 1 MeV. Based on these results, we also predict parity inversion for ^{13}Be ; experimentally, the parity of the ground state is not confirmed, though likely to be negative [26], which indeed implies parity inversion (^{13}Be has one neutron in the sd -shell, so the natural parity is positive).

It is not yet clear whether the relative underbinding of the unnatural parity states compared to the natural parity states in beryllium is a deficiency of the NN interaction, JISP16, or due to underestimating the numerical error in the extrapolation to the infinite basis, in particular for the unnatural parity states [27]. Also the general underbinding of the ground states hints at a deficiency of JISP16. Indeed, it is unlikely that this interaction is 'perfect': it was fitted to the NN scattering data, as well as to select observables in light nuclei, in particular to ^6Li . Nevertheless, the overall agreement between data and our calculation is quite encouraging, and we expect to be able to get even closer to the data with improved NN and 3NF potentials.

For a true ab initio calculation one would obtain the nuclear forces (NN, 3NF, etc.) from the underlying quantum field theory, QCD. Unfortunately, that is not yet possible without introducing free parameters. Based on QCD, one can derive nonrelativistic effective NN, 3NF, and even 4NF nuclear potentials using chiral perturbation theory (ChPT) [2, 4]. Such a derivation determines the structure of the nuclear interaction, but not the numerical constants

that govern the strength of the different terms in the interaction – these have to be fitted to low-energy nuclear physics data. (In the future they may be calculable through lattice QCD.)

4. Understanding the Gamow–Teller transitions between ^{14}C and ^{14}N

The anomalously long lifetime of ^{14}C , 5730 ± 30 years, compared to lifetimes of other light nuclei undergoing the same decay process, allowed Gamow–Teller (GT) beta-decay, poses a major challenge to ab initio nuclear structure calculations. Not only is the number of particles (14) pushing the limit of what ab initio calculations can reliably calculate, the experimental lifetime can only be reproduced by an anomalously small matrix element for this transition. This suggests that delicate cancellations could play a crucial role, which always poses a challenge to numerical calculations. On the other hand, since the transition operator, in leading approximation, depends only on the nucleon spin and isospin but not on the spatial coordinate, this decay provides a precision tool to inspect selected features of the initial and final states.

Traditional realistic NN forces alone appear insufficient to produce the observed lifetime [28, 29], indicating that three-body forces may be needed. Indeed, in Ref. [21] we showed that the $3NF$ of ChPT plays a major role in producing a transition rate that is near zero, needed for the anomalous long lifetime. We used the chiral two- and three-body potentials of ChPT [2, 4] and the No-Core Shell Model (NCSM) using Lee–Suzuki (LS) renormalization [30] to improve the convergence. The non-perturbative coupling constants of the 3-body force, not fixed by $\pi - N$ or NN data, are c_D for the $N - \pi - NN$ contact term and c_E for the $3NF$ contact term. In Ref. [21] we presented results for $(c_D, c_E) = (-0.2, -0.205)$ and for $(-2.0, -0.501)$. Both sets fit the $A=3$ binding energies and are allowed by the ‘naturalness criterium’ for these parameters. The former also produces a precise fit to the triton half life [31]; the latter produces the triton half life within 20% of experiment but is preferred by the ^{14}C half life.

In the left panel of Fig. 8 we show the obtained binding energy of ^{14}N both with the chiral two- and three-body forces and with the phenomenological two-body interaction JISP16. For JISP16 we can use our extrapolation technique to extract the binding energy in the complete basis space: we find 116(5) MeV, that is, ^{14}N is overbound by about 10 MeV with JISP16. For the chiral two- and three-body forces we used a LS renormalization procedure on the truncated basis space, which means that the results are no longer variational upperbounds, and the convergence

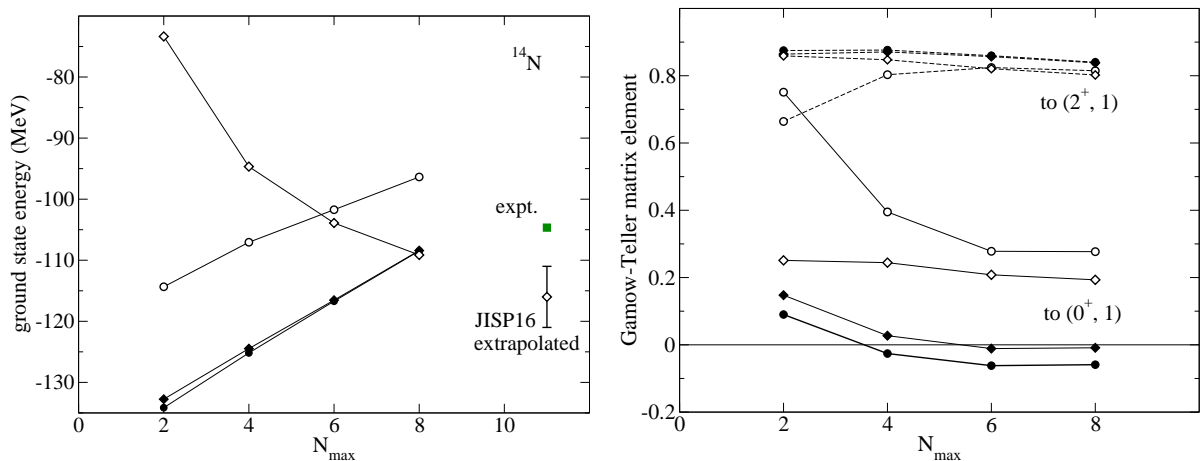


Figure 8. Ground state energies of ^{14}N (left) and GT matrix element (right) as function of N_{max} with JISP16 at $\hbar\omega = 27.5$ MeV (\diamond), with chiral two-body forces at $\hbar\omega = 14.0$ MeV (\circ), with chiral two- and three-body forces at $\hbar\omega = 14.0$ MeV with $(c_D, c_E) = (-0.2, -0.205)$ (\bullet) and with $(c_D, c_E) = (-2.0, -0.501)$ (\blacklozenge), and experimental data (\blacksquare).

to the infinite basis space is not monotonic. Our results for the binding energy do not imply convergence with N_{\max} ; however, the obtained spectrum at $N_{\max} = 8$ appears to be reasonably well converged [21] and in qualitative agreement with the experimental spectrum, both for ^{14}C and for ^{14}N . Furthermore, in general the LS ground state energies increase with N_{\max} at small and moderate N_{\max} values, but this trend tends to turn around at (very) large N_{\max} values, and in the limit $N_{\max} \rightarrow \infty$ the ground state energy tends to converge from above, as is the case without LS renormalization.

The GT matrix element that governs the β -decay of ^{14}C is

$$M_{\text{GT}} = \sum_{\alpha, \beta} \langle \beta | \sigma \tau_+ | \alpha \rangle \rho_{\alpha\beta}, \quad (11)$$

where $\langle \alpha | \sigma \tau_+ | \beta \rangle$ is the one-body matrix element between HO single-particle states α and β , which is non-vanishing only when both single-particle states are in the same shell, and the one-body density matrix

$$\rho_{\alpha\beta} \equiv \langle \Psi_f | a_\beta^\dagger a_\alpha | \Psi_i \rangle, \quad (12)$$

with $\langle \Psi_f |$ and $| \Psi_i \rangle$ the ^{14}N and ^{14}C ground states respectively. For comparison, we also calculate the GT transition between the first 2^+ state in ^{14}C and the ground state in ^{14}N . In order to reproduce the measured half life of $T_{1/2} \simeq 5730$ years, the GT matrix element must be anomalously small, $|M_{\text{GT}}^M| \simeq 2 \times 10^{-3}$, in contrast with a conventional strong GT transition between states in light nuclei with $|M_{\text{GT}}| \simeq 1$.

In the right panel of Fig. 8 we show GT matrix elements³ both with the chiral two- and three-body forces and with JISP16. The results for the GT matrix element between the ground state of ^{14}N and the lowest $(J^\pi, T) = (2^+, 1)$ excited state of ^{14}C is reasonably well converged for the different interactions. Furthermore, it is insensitive to the interaction: JISP16 gives approximately the same result as the chiral interaction, with or without 3-body forces. Our calculations are in reasonable agreement with experiment: the measured transition rate from the ground state in ^{14}N to the low-lying 2^+ states in ^{14}C is $\sum B(GT) = 0.92(33)$ [29], compared to our calculated value for the transition rate of about 1.6.

The situation is very different for the GT matrix element between the ground state of ^{14}N and the $(0^+, 1)$ ground state of ^{14}C . The results with JISP16 do not depend much on the basis space truncation, and the matrix element is suppressed compared to a 'natural' value of the order of one, but not sufficiently suppressed in order to explain the long lifetime of ^{14}C . The results with the chiral NN forces alone depend much stronger on N_{\max} , but they do seem to be converged at $N_{\max} = 8$, also at a value that is significantly smaller than the 'natural' value of one, but not sufficiently suppressed in order to explain the long lifetime of ^{14}C . However, once we add the chiral 3NF, we do get a further suppression of the GT matrix element to almost zero, depending on the exact values of (c_D, c_E) .

In order to reveal what drives this suppression, we show in Fig. 9 the decomposition of M_{GT} at $N_{\max} = 8$ into the contributions arising from each HO shell for two cases with the 3NF ($c_D = -0.2, -2.0$) and one without. On the left we show our results for the transition between the ground states of ^{14}N and ^{14}C (corresponding to β -decay of ^{14}C); on the right the transition between the ground state of ^{14}N and the first excited 2^+ state of ^{14}C . The largest effect occurs in the p -shell for the transition between the ground states of ^{14}N and ^{14}C , where the 3NF reduces the contributions by an order-of-magnitude from the result with the NN interactions only. This happens for both values of c_D ; also note that the transition between the ground state of ^{14}N and

³ For simplicity, these results are obtained by calculations by assuming isospin symmetry in ^{14}N , and considering transitions between the $(1^+, 0)$ ground state and the lowest $(0^+, 1)$ and $(2^+, 1)$ excited states in ^{14}N .

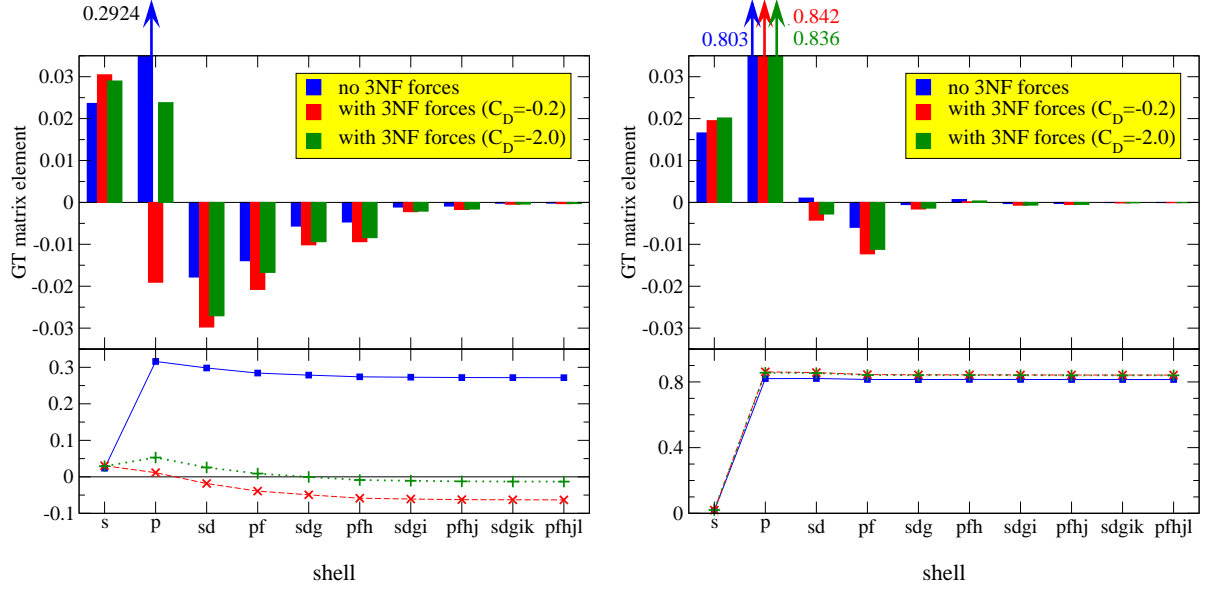


Figure 9. GT matrix element for the transitions ^{14}N to the 0^+ (left) and 2^+ (right) states of ^{14}C , decomposed per HO shell, obtained with two-body chiral interaction with (red and green) and without (blue) three-body forces (3NF) at $N_{\text{max}} = 8$. Top panels display the contributions summed within the shell to yield a total for that shell. Bottom panels display the running sum of the GT contributions over the shells included in the sum. Note that the top panels have the same scale left and right, but the bottom panels do not.

the first excited 2^+ state of ^{14}C receives its largest contribution from the p -shell, and is barely affected by the 3NF. In addition, the three-body forces significantly enhance the contributions of each of the higher shells, for both transitions. In combination with the strong cancellations within the p -shell for the GT matrix element between the ground states of ^{14}N and ^{14}C , the contributions of the higher shells overwhelm that of the p -shell, whereas these higher shells contribute almost nothing to the value of the GT matrix element between the ground state of ^{14}N and the first excited 2^+ state of ^{14}C .

Finally, we calculated the GT matrix element using one wavefunction obtained with three-body forces, but the other wavefunction obtained without three-body forces. Fig. 10 clearly shows that it is the $(1^+, 0)$ ground state of ^{14}N , rather than the $(0^+, 1)$ ground state of ^{14}C , that causes the cancellations within the p -shell once the three-body forces are included. This seems to be a recurring theme of three-body forces in the p -shell nuclei – they manifest themselves in particular in the odd-odd nuclei [5].

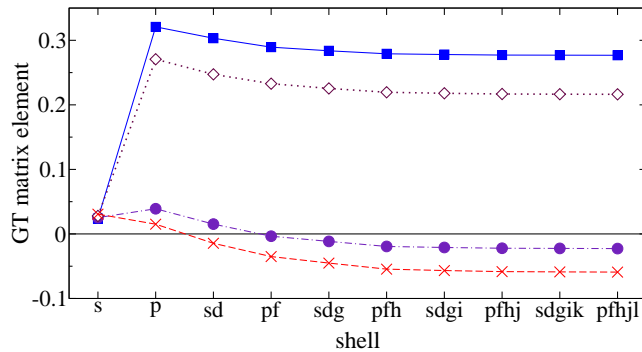


Figure 10. M_{GT} between the ground states of ^{14}N and ^{14}C , using the ^{14}N wavefunction obtained with 3NF, but the ^{14}C wavefunction obtained without 3NF (purple \bullet), and vice versa (maroon \diamond). For comparison, we also include the results with (red cross) and without (blue \blacksquare) 3NF for both wavefunctions.

Of course, the precise value of the strongly suppressed GT matrix element between the ground states of ^{14}N and ^{14}C depends on details of the interaction, of the operator, and of the calculations, because of the cancellations between the dominant contributions. Although meson-exchange currents do not contribute significantly to GT transition with a 'natural' value of the order of one [32], they may be important for the actual value of anomalously long lifetime of ^{14}C . For a purely phenomenological interaction like JISP16 it is unclear what the appropriate corrections to the canonical operator would be; but with the chiral interactions one should use consistent meson-exchange currents, and apply the same renormalization procedure to the operators as to the interaction. These effects are currently under investigation.

Acknowledgments

We would like to thank Takashi Abe, Mark Caprio, Chase Cockrell, and James Vary for useful discussions. This work was supported in part by U.S. Department of Energy Grant DE-FC02-09ER41582 (SciDAC/UNEDF) and DE-FG02-87ER40371, and by the U.S. NSF grant 0904782. Computational resources were provided by the National Energy Research Supercomputer Center (NERSC), which is supported by the DOE Office of Science, and by an INCITE award, "Nuclear Structure and Nuclear Reactions", from the DOE Office of Advanced Scientific Computing. This research used resources of the Oak Ridge Leadership Computing Facility at ORNL, which is supported by the DOE Office of Science under Contract DE-AC05-00OR22725.

References

- [1] Wiringa R B, Stoks V G J and Schiavilla R 1995 *Phys. Rev.* **C51** 38
- [2] Entem D R and Machleidt R 2003 *Phys. Rev.* **C68** 041001
- [3] Pieper S C, Pandharipande V R, Wiringa R B and Carlson J 2001 *Phys. Rev.* **C64** 014001
- [4] Epelbaum E 2006 *Prog. Part. Nucl. Phys.* **57** 654–741
- [5] Navratil P, Gueorguiev V G, Vary J P, Ormand W E and Nogga A 2007 *Phys. Rev. Lett.* **99** 042501
- [6] Bertsch G F, Dean D J and Nazarewicz W 2007 *SciDAC Review* **6** 42
- [7] Furnstahl R J (for the UNEDF Council) 2011 *Nuclear Physics News* **21** 18
- [8] Nam H *et al.* 2012 *these proceedings (Preprint 1205.227)*
- [9] Cockrell R, Maris P and Vary J P 2012 *Phys. Rev.* **C86** 034325 (*Preprint 1201.0724*)
- [10] Caprio M A, Maris P and Vary J P 2012 *Phys. Rev.* **C86** 034312 (*Preprint 1208.4156*)
- [11] Gloeckner D and Lawson R 1974 *Phys. Lett.* **B53** 313
- [12] Abe T, Maris P, Ostuka T, Shimizu N, Utsuno Y and Vary J 2011 *AIP Conf. Proc.* **1355** 173
- [13] Abe T, Maris P, Otsuka T, Shimizu N, Utsuno Y and Vary J 2012 *Phys. Rev. C* in press (*Preprint 1204.1755*)
- [14] Shirokov A M, Vary J P, Mazur A I and Weber T A 2007 *Phys. Lett.* **B644** 33
- [15] Maris P, Vary J P and Shirokov A M 2009 *Phys. Rev.* **C79** 014308
- [16] Bogner S K, Furnstahl R J, Maris P, Perry R J, Schwenk A and Vary J P 2008 *Nucl. Phys.* **A801** 21
- [17] Sternberg P, Ng E G, Yang C, Maris P, Vary J P, Sosonkina M and Le H V 2008 *Proc. of the 2008 ACM/IEEE conference on Supercomputing* (Piscataway, NJ, USA: IEEE Press) pp 15:1–15:12 ISBN 978-1-4244-2835-9
- [18] Vary J P, Maris P, Ng E, Yang C and Sosonkina M 2009 *J. Phys. Conf. Ser.* **180** 012083
- [19] Maris P, Sosonkina M, Vary J P, Ng E and Yang C 2010 *Procedia Computer Science* **1** 97
- [20] Srinivasa S, Sosonkina M, Maris P, and Vary J P 2012 *Procedia Computer Science* **9** 256
- [21] Maris P Vary J P, Navratil P, Ormand W E, Nam H, and Dean D J 2011 *Phys. Rev. Lett.* **106** 202502
- [22] Bohlen H G *et al.* 2008 *J. Phys.: Conf. Ser.* **111** 012021
- [23] Rowe D J 1970 *Nuclear Collective Motion* (London: Methuen, London)
- [24] Caprio M A, Maris P and Vary J P 2012 *in preparation*
- [25] Tilley D, Kelley J, Godwin J, Millener D, Purcell J, Sheu C and Weller H 2004 *Nuclear Physics A* **745** 155
- [26] Audi G, Bersillon O, Blachot J and Wapstra A 1997 *Nuclear Physics A* **624** 1
- [27] Forssen C, Navratil P, Ormand W E and Caurier E 2005 *Phys. Rev.* **C71** 044312
- [28] Aroua S *et al.* 2003 *Nucl. Phys.* **A720** 71
- [29] Negret A *et al.* 2006 *Phys. Rev. Lett.* **97** 062502
- [30] Suzuki K and S. Y. Lee S Y 1980 *Prog. Theor. Phys.* **64** 2091; Suzuki K 1982 *Prog. Theor. Phys.* **68**, 246; **68** 1999; Suzuki K and Okamoto R (1994) *Prog. Theor. Phys.* **92** 1045
- [31] Gazit D, Quaglioni S and Navratil P 2009 *Phys. Rev. Lett.* **103** 102502
- [32] Vaintraub S, Barnea N and Gazit D 2009 *Phys. Rev.* **C79** 065501